Computer-Aided Generation of Nonlinear Reduced-Order Dynamic Macromodels—I: Non-Stress-Stiffened Case

Lynn D. Gabbay, Jan E. Mehner, and Stephen D. Senturia, *Fellow, IEEE*

***Abstract*—Reduced-order dynamic macromodels are an effective way to capture device behavior for rapid circuit and system simulation. In this paper, we report the successful implementation of a methodology for automatically generating reduced-order nonlinear dynamic macromodels from three-dimensional (3-D) physical simulations for the conservative-energy-domain behavior of electrostatically actuated microelectromechanical systems (MEMS) devices. These models are created with a syntax that is directly usable in circuit- and system-level simulators for complete MEMS system design. This method has been applied to several examples of electrostatically actuated microstructures: a suspended clamped beam, with and without residual stress, using both symmetric and asymmetric positions of the actuation electrode, and an elastically supported plate with an eccentric electrode and unequal springs, producing tilting when actuated. When compared to 3-D simulations, this method proves to be accurate for non-stress-stiffened motions, displacements for which the gradient of the strain energy due to bending is much larger than the corresponding gradient of the strain energy due to stretching of the neutral surface. In typical MEMS structures, this corresponds to displacements less than the element thickness. At larger displacements, the method must be modified to account for stress stiffening, which is the subject of part two of this paper. [448]**

***Index Terms*—Basis-function methods, computer-aided design, electrostatic actuation, energy methods, macromodels, modal analysis, reduced-order models.**

I. Introduction

MICROELECTROMECHANICAL systems (MEMS) typically involve multiple energy domains, such as kinetic energy, elastic deformation, electrostatic or magnetostatic stored energy, and fluidic interactions. There is great value in being able to capture the complex multi-energy-domain physics into relatively compact dynamic models (implemented, e.g., with a few coupled ordinary differential equations) so that dynamic simulation at the circuit and system level can be done rapidly, without solving coupled partial differential equations at every time step. Such compact models are variously referred to as *macromodels* or, because of the relatively few dynamic degrees of freedom, *reduced-order models*.

In a recent review of this subject [1], the following desirable attributes for a macromodel were enumerated: analytical (rather than numerical), correct dependence on device dimensions and material properties, correct energy behavior (energy conserving where appropriate, entropy producing when dissipative), able to describe both quasi-static and dynamic behavior for both small (linear) and large (presumably nonlinear) motions and, most importantly, quantitative agreement with the results of full three-dimensional (3-D) physical simulation and with experiments on a suitable set of test structures. In practice, macromodels used by designers today meet some, but not all, of these criteria and, typically, these models are hand-built for each specific device.

We have been exploring methods to automate the construction of nonlinear macromodels directly from physical-level simulation. In this two-part paper sequence, we present an approach that uses basis-function methods; a subject with a long history (see below). This paper uses the linear elastic normal modes of a device as a basis set, and reports the development of automated procedures for constructing dynamic macromodels that accurately capture such nonlinear effects as electrostatic spring softening and mode coupling. However, it is found that this approach is limited to non-stress-stiffened motions, which, for elastic bodies, are displacements for which the gradient of the strain energy due to bending is much larger than the corresponding gradient of the strain energy due to stretching of the neutral surface. In typical MEMS structures, this corresponds to displacements less than the element thickness. When the motions are larger, stress stiffening causes the normal modes to fail as a good basis set. Part two of this paper [2] addresses the stress-stiffening issue and reports a modified basis-function approach that appears to give extremely good results for an interesting class of MEMS devices.

Much of the difficulty in modeling MEMS devices derives from the tight coupling between the multiple energy domains. Individual physical effects (elasticity or fluid mechanics) are governed by partial differential equations, typically nonlinear. When these equations become coupled, e.g., through the elastic deformation of a structure that simultaneously serves as a plate

Manuscript received May 18, 1999; revised November 29, 1999. This work was supported by the Defense Advanced Research Projects Agency Microsystems Technology Office Microelectromechanical Systems Program under Contract J-FBI-95-215. Subject Editor, K. D. Wise.

L. D. Gabbay was with the Microsystems Technology Laboratories, Massachusetts Institute of Technology, Cambridge, MA 02139 USA. He is now at 1301 Shoreway Road, Belmont, CA 94002 USA (e-mail: ldgabbay@alum.mit.edu).

J. E. Mehner was with the Microsystems Technology Laboratories, Massachusetts Institute of Technology, Cambridge, MA 02139 USA. He is now with the Chemnitz University of Technology, Chemnitz D-09107, Germany (e-mail: mehner@infotech.tu-chemnitz.de).

S. D. Senturia is with the Microsystems Technology Laboratories, Massachusetts Institute of Technology, Cambridge, MA 02139 USA (e-mail sds@mit.edu).

Publisher Item Identifier S 1057-7157(00)04853-8.

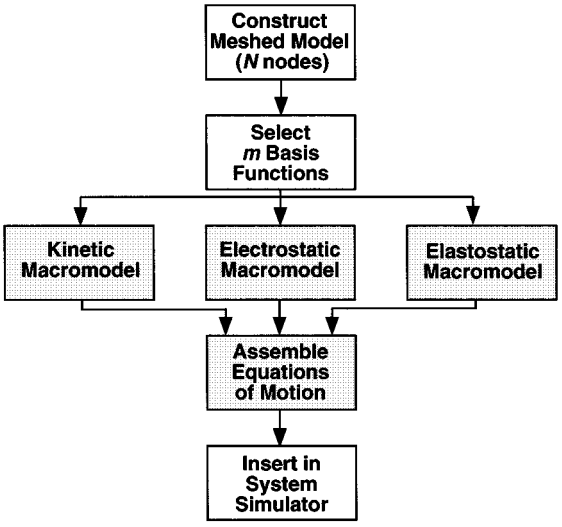

Fig. 1. Overview of automated macromodeling process.

of a capacitor and the boundary of a compressed fluid, the computational challenges of highly meshed numerical simulation become formidable. There has been some success in coupled quasi-static simulation, and in the development of fast solvers for individual energy domains (see discussions in [1], [3], and [4]), but nonlinear dynamic simulation in such coupled systems is too cumbersome for rapid system-level simulation of device and circuit behavior. This is especially critical when one seeks to close a feedback loop around a device; compact yet accurate dynamical models are essential in such cases.

Section II introduces the requisite background on basis-function methods. There follows a step-by-step discussion (with examples) of our automated method for building macromodels based on selected linear normal modes as basis functions. This paper concludes with a brief discussion of the stress-stiffening problem, which is taken up in detail in [2].

II. Theoretical Approach

Fig. 1 shows a schematic view of the automated macromodeling process [5]. Starting with a meshed device model with N nodes, $3N$ spatial degrees of freedom, and $6N$ dynamical state variables, we construct a lower order representation with only m degrees of freedom (with $m \ll N$), and using energy methods, construct analytical macromodels for the kinetic energy, the elastostatic energy, and the electrostatic energy in terms of a suitably selected set of generalized coordinates for the device. Gradients of the energy functions, which can be calculated symbolically, then yield the dynamical equations of motion, which, in the method presented here, are constructed in a format that is directly insertable into a system-level simulator.

Recall that the Lagrangian $L(q,\, \dot{q},\, t)$ is a function of the general coordinates q, their first-time derivatives $\dot{q}$, and time t. $L(q,\, \dot{q},\, t)$ is defined by

$$L(q,\, \dot{q},\, t) = T(q,\, \dot{q},\, t) - U(q,\, \dot{q},\, t) \tag{1}$$

where $T(q,\, \dot{q},\, t)$ is the kinetic energy and $U(q,\, \dot{q},\, t)$ is the potential energy of the system [6]. The equations of motion come directly from Lagrange's equations, given by

$$\frac{d}{dt}\left(\frac{\partial L}{\partial \dot{q}_i}\right) - \frac{\partial L}{\partial q_i} = 0. \tag{2}$$

There are m equations of this form, one for each generalized coordinate q_i.

A. Normal Modes as Basis Functions

In this paper, we choose q_i to be the time-dependent amplitudes of a set of basis functions. We begin with the nodal displacements $u(r,\, t)$, a $3N$-element vector, written in the form

$$u(r,\, t) = u_{\text{eq}} + \sum_{i=1}^{m} q_i(t)\varphi_i(r) \tag{3}$$

where q_i is the time-dependent amplitude of the basis function $\varphi_i(r)$, and the sum is over m basis functions (where $m \ll N$). The term u_{eq} is included to account for possible relaxation of initial stress following release of the MEMS structure, and represents the equilibrium (unforced) position of the system.

The elastic linear normal modes provide an attractive set of candidate basis functions (see, e.g., [7]). The dynamical equations for the device, written in terms of u's, are

$$[M]\,\frac{d^2u}{dt^2} + F_m(u,\, t) - F_e(u,\, t) = 0 \tag{4}$$

where $[M]$ is the usual mass matrix defined on the mesh (presumed to be time independent), F_m is the nodally defined elastostatic force

$$F_{m,\,i}(u,\, t) = \frac{\partial U_m(u,\, \dot{u},\, t)}{\partial u_i} \tag{5}$$

and F_e is the nodally defined electrical force

$$F_{e,\,i} = \frac{\partial U_e^*(u,\, \dot{u},\, t)}{\partial u_i} \tag{6}$$

where, for electrostatic actuation, the co-energy U_e^* is used instead of the energy (presuming voltage control rather than charge control), and the corresponding force term carries an additional minus sign [8].

For small-amplitude displacements, F_m can be linearized to yield

$$[M]\,\frac{d^2u}{dt^2} + [K]u = F_e(u,\, t) \tag{7}$$

where $[K]$ is the usual stiffness matrix, which is the (time-independent) Jacobian of F_m when the device is in its equilibrium position. For the set of linear problems (no stress stiffening), the representation with $[K]$ is exact, and the left-hand side can be readily diagonalized. The resulting eigenvectors are the linear mode shapes for the device from which we will select our basis functions $\varphi_i(r)$. For convenience in implementing the macromodels, we choose to normalize the basis functions to unit

maximum amplitude. The q_i's then provide a direct measure of modal contribution. The resulting dynamical equations become

$$[M_G]\frac{d^2q}{dt^2} + [K_G]q = F_e(q, t) \tag{8}$$

where $[M_G]$ is the global mass matrix, $[K_G]$ is the global stiffness matrix, and, in making this transformation to basis functions, we now require that the electrostatic force $F_e(q, t)$ be expressed in terms of the basis-function amplitudes q rather than the nodal displacements u. Truncating this set of equations to m generalized coordinates accomplishes the desired model-order reduction.

B. Kinetic and Elastic Energy

The advantage of using linear normal modes as basis functions is immediately obvious. Both $[M_G]$ and $[K_G]$ are diagonal matrices. If M_i is the global-mass-matrix entry for the ith mode, the corresponding entry in the global stiffness matrix becomes $M_i\omega_i^2$, where ω_i is the undamped resonance frequency of the ith mode. Connecting back to the Lagrangian picture, we can immediately write

$$T(q, \dot{q}, t) = \sum_i \frac{1}{2} M_i \dot{q}_i^2 \tag{9}$$

and

$$U_m(q, \dot{q}, t) = \sum_i \frac{1}{2} M_i \omega_i^2 q_i^2. \tag{10}$$

Thus, two of the three required energy functions are trivially obtained when we use normal modes for basis functions. Anathasuresh [9] has already demonstrated this approach for electrostatic actuation, including mode-coupling and spring-softening effects, but he required that the electrostatic force be evaluated in u space rather than q space, necessitating two transformations between the u's and q's at each time step, and an evaluation of F_e on the N mesh rather than in the smaller q space. Our approach is to generate an accurate analytic form of $U_e^*(q)$ directly in q space, from which the electrostatic force in q space is then obtained by differentiation.

C. Electrostatic Co-Energy

In order to construct the electrostatic co-energy $U_e^*(q)$, it is necessary to determine which modes will contribute significantly to the device behavior, and what range of amplitude must be considered for each important mode. Our approach begins with a single static coupled-energy-domain 3-D quasi-static simulation for the device under a typical example of actuation. Let $u_{\rm ex}$ be the positional state calculated from this quasi-static simulation. It is possible (e.g., with least squares via the QR factorization algorithm [10]) to determine the coefficients c_i that constitute the best representation of the form

$$u_{\rm ex} = u_{\rm eq} + \sum_{i=1}^{m'} c_i \varphi_i \tag{11}$$

where m' is the total number of modes being tested (typically fewer than 30). If we assume that $u_{\rm ex}$ is an example of typical

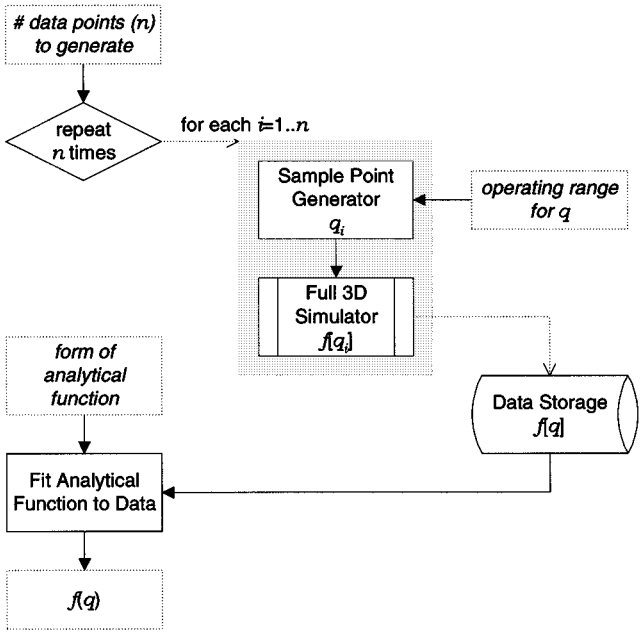

Fig. 2. Macromodeling algorithm for 3-D simulations in q space.

motion, then a sorted list of mode shapes in decreasing order of contribution identifies which modes are important, and to what degree. The designer can use this information to select the number of basis functions m to include in the macromodel (in the examples to follow, the most complex case used only five basis functions). Furthermore, the magnitudes of the coefficients c_i are used to predict the relative expected magnitudes of the q_i during device operation and, thus, serve to estimate the extent of q space that must be covered when constructing $U_e^*(q)$.

Once the specific mode selection is completed and the estimated relative modal amplitudes c_i are found, the procedure for generating $U_e^*(q)$ is illustrated in Fig. 2. Recall that the electrostatic co-energy is defined as

$$U_e^*(q) = \frac{1}{2} C(q) V^2 \tag{12}$$

where V is the voltage on the actuation capacitor. Since under voltage-controlled conditions the applied voltage is independent of motion, the gradient need only be applied to the capacitance, thus

$$F_e = \left(\frac{1}{2} V^2\right) \nabla C. \tag{13}$$

Full 3-D capacitance simulation is run several times for values of the generalized coordinates that adequately span the predetermined operating range for the device.[1] We then select a rational fraction of multivariate polynomials to represent the capacitance function, and use the Levenberg–Marquardt nonlinear function fitting scheme [11] to find the parameters that best fit this generalized form. Recall that the capacitance of a large parallel-plate capacitor neglecting fringe field effects is given by $\varepsilon_0 A/d$, where A is the area of the plate and d is the distance between the plates. Our generalized coordinates would

[1]The sample point generator in Fig. 2 is based on an algorithm that efficiently selects a set of well-spaced random points to fill the selected q space. Details and the source code are available in [5].

most closely correspond to a change in the gap d. Thus, it makes sense that our analytical form should have denominator terms in addition to numerator terms. The specific form is

$$C(q) = \frac{\sum_{i_1=0}^{R_1} \sum_{i_2=0}^{R_2} \cdots \sum_{i_m=0}^{R_m} a_{i_1 i_2 \cdots i_m} q_1^{i_1} q_2^{i_2} \cdots q_m^{i_m}}{\sum_{i_1=0}^{S_1} \sum_{i_2=0}^{S_2} \cdots \sum_{i_m=0}^{S_m} b_{i_1 i_2 \cdots i_m} q_1^{i_1} q_2^{i_2} \cdots q_m^{i_m}}. \quad (14)$$

The designer must specify the order of terms for each basis function, after which the generation of simulations and the fitting procedures are done automatically. For convenience in labeling the complexity of the capacitance fitting function, we shall refer to (14) as a model with the label

$$[\, R_1 \quad R_2 \quad \cdots \quad R_m / S_1 \quad S_2 \quad \cdots \quad S_m \,]. \quad (15)$$

This same approach can be applied to other energy domains, but only if the selected mode shapes yield good estimates of the relevant energy function. In the case of elastic deformation, e.g., it will be shown in [2] that the linear normal modes fail to capture the stress-stiffened elastic energy function. However, Varghese [12] has recently applied this method to Lorentz-force magnetic actuation with good results.

D. Assembling the Equations of Motion

We now combine the macromodels for the kinetic, electrostatic, and elastostatic energy domains. Using the kinetic-domain representation from (9), the elastic-domain representation from (10), and the electrostatic-domain representation from (14), and correctly accounting for the use of electrostatic co-energy instead of energy, our equations of motion become

$$M_i \ddot{q}_i + M_i \omega_i^2 q_i = \frac{1}{2} V(t)^2 \frac{\partial C(q)}{\partial q_i}. \quad (16)$$

Since our representation of the capacitance $C(q)$ is an analytical function, we can compute the gradient of this function analytically rather than numerically. This avoids the possibility of numerical errors creating hidden energy sources or sinks, thereby creating or destroying energy arbitrarily within our equations of motion.

Finally, the resulting equations of motion are written to an analog hardware description language input file.[2] Note that all data extraction, macromodel generation, equation of motion assembly, and input file exportation are done automatically by computer. The initial investment of time to generate the macromodel in the form of a circuit-simulator input file need only be made once. This input file may then be used repeatedly for any number of dynamic simulations, including systems with feedback.

III. Examples and Results

Let us walk through the steps of the automated macromodeling process for a mechanically nontrivial example. We choose a 125 × 155 × 3 μm plate suspended by four 85 × 15 μm beams. Two of the beams are 3-μm thick, one is 2-μm thick, and one is 1-μm thick. At the corner with the weakest support beam, a 62.5 × 70 μm electrode is placed underneath, separated from the plate by a 4-μm gap. This device is made out of polysilicon with a Young's modulus of 165 GPa and a Poisson ratio of 0.23. Due to the unequal beam thicknesses and the off-centered electrode, this structure displaces, bends, and tilts upon actuation with a voltage.

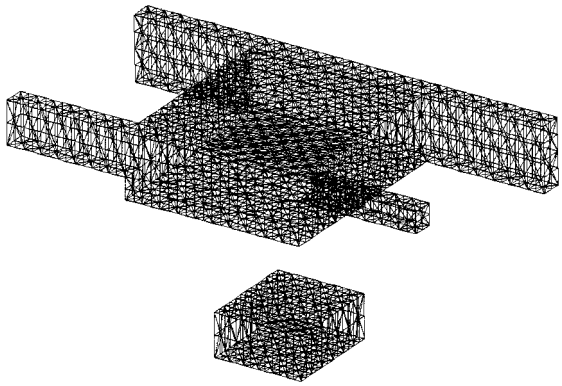

Fig. 3. Example: asymmetric suspended plate with unequal support beams and an off-center actuation electrode.

The results presented here were computed on a Sun Ultra-1 Model 170 workstation with 196-Mb RAM running SunOS 5.5. Microcosm MEMCAD,[3] in conjunction with ABAQUS[4] and FastCap [16] was used to execute full 3-D simulation. SABER was used to execute the circuit simulation of the resulting macromodeled equations of motion. All the remaining steps were computed with a tool suite collectively referred to as the CHURN process. Full details and source codes for CHURN are available in [5].

We first construct a solid model using the MEMCAD system, and mesh it to create the finite-element model (FEM) of the structure. Fig. 3 depicts the FEM with the perpendicular axis magnified 20× for clarity. The FEM is comprised of 318 20-node brick elements, with a total of 2814 nodes.

We then execute a single quasi-static coupled simulation using CoSolve-EM (part of MEMCAD). We select a voltage of 100 V, which is 61% of the pull-in voltage for this structure. This required four relaxation iterations to converge, requiring 7.5 min to compute. The resulting deformation is depicted in Fig. 4.

Next, we determine the first 30 mode shapes for this device using the modal-analysis feature of ABAQUS (embedded within MEMCAD). This required 11.6 min to compute. We now project the quasi-static solution onto the mode shapes using the QR factorization module of the CHURN package. Table I identifies the ten most significant modes contributing to this deformation in decreasing order of contribution magnitude, rounded to two significant figures.

Fig. 5 shows the five mode shapes that were selected to be used as basis functions. Table II presents the calculated information about each of these modes.

[2]The specific format is for the SABER System (Analogy Inc., Beaverton, OR. [Online]. HTTP: http://www.analogy.com). Modification for other analog hardware description languages is straightforward.

[3]Microcosm Technologies, Cambridge, MA. http://www.memcad.com

[4]Hibbitt, Karlsson, and Sorensen Inc., Pawtucket, RI. http://www.hks.com

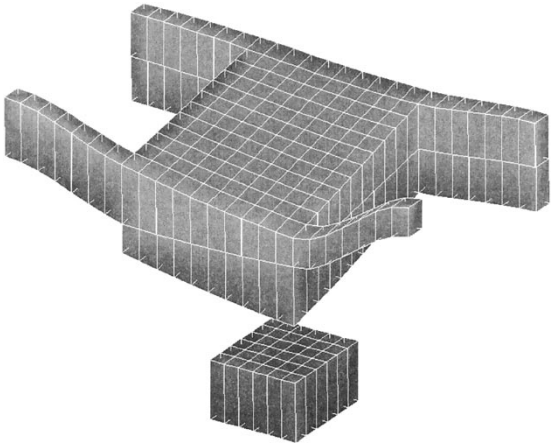

Fig. 4. Quasi-static response of asymmetric suspended plate with 100-V actuation.

TABLE I
PROJECTION OF QUASI-STATIC RESPONSE OF FIG. 4 ONTO MODE SHAPES

mode #	contribution
1	-0.46
2	0.042
3	0.025
7	0.0057
4	-0.0052
8	-0.0012
6	0.00090
10	-0.00070
14	0.00050
15	-0.00049

Using the CHURN procedure of Fig. 2, we perform 250 capacitance calculations that span the required portion of q space and fit a $[43322/32211]$ multivariate polynomial fraction, which has 863 fitting parameters. The resulting $\chi^2 = 4.30 \times 10^{-5}$. The capacitance computations required 1.9 h; the analytical fit and gradient computation to yield $F_e(q)$ required 30.7 min.

In Figs. 6 and 7, we present examples of system-level dynamic simulations of our macromodel for this structure. On average, these took 2 min to compute. In Fig. 6, we observe that the relatively large response of Mode 1 to the sawtooth waveform appears as a quasi-static peak in the other modes, followed by characteristic ringing in each mode when the load is quickly removed. This demonstrates that nonlinear mode coupling is captured by the macromodel. In Fig. 7, we observe complex modal waveforms depending on the exact timing of the square pulses with the phase in each mode.

Figs. 8–10 depict three other example structures, which we macromodeled using this automated process in order to develop some timing and performance metrics. In all three cases, the material constants were the same: Young's modulus of 165 GPa and a Poisson ratio of 0.23. In Table III, we summarize and compare the key statistics for all four structures and, in Fig. 11, we present a comparison of macromodeling computation times. We note that even the most complex example took only a few hours for complete macromodel construction.

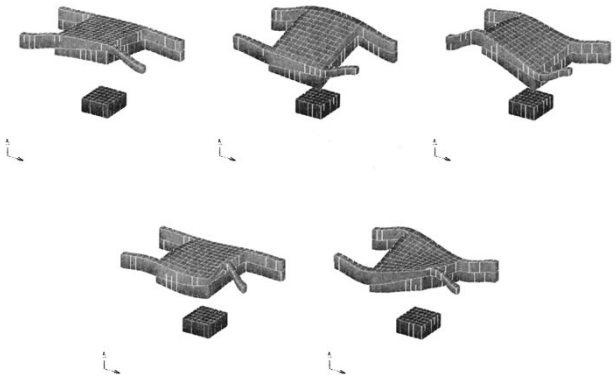

Fig. 5. Mode shapes used to comprise basis set.

TABLE II
MODAL MASSES, RESONANT FREQUENCIES, AND STIFFNESSES

Mode Number	Mass (kg)	Frequency (Hz)	Stiffness (N/m)	Period (μs)
1	4.34E-11	121	25.1	8.26
2	3.54E-11	273	104.2	3.66
3	3.14E-11	424	222.9	2.36
4	1.19E-11	931	407.3	1.07
7	1.54E-12	1,267	97.4	0.79

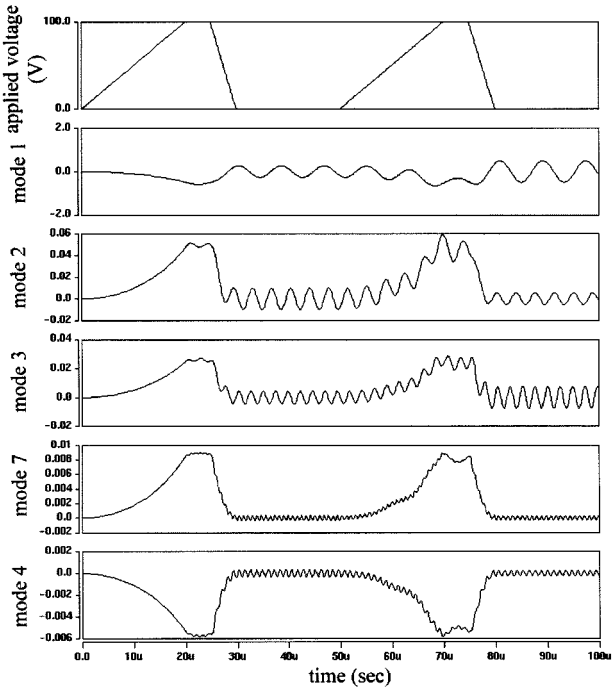

Fig. 6. Response to a 100-V sawtooth wave with 20-μs rise, 5-μs hold, and 50-μs period.

IV. COMPARISON TO QUASI-STATIC ANALYSIS

An important issue is the accuracy of the extracted macromodel. The most direct comparison is to simulate dynamical transients using the macromodel and explicit FEM calculations. This kind of comparison is shown and discussed in [2]. Another comparison is to take the dynamical equations of motion and set the time derivatives to zero (the quasi-static case). The result is a set of coupled algebraic equations whose solution should agree with the quasi-static meshed simulation using CoSolve-EM over

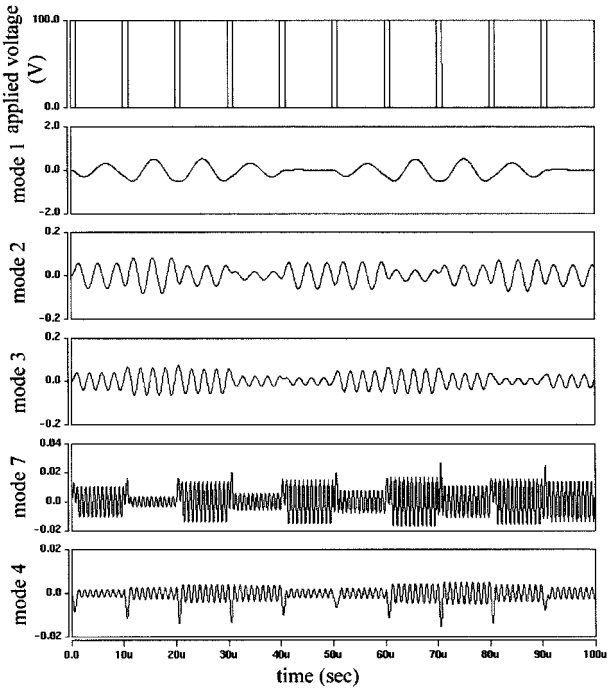

Fig. 7. Response to a 100-V square wave with 1-μs hold and 10-μs period.

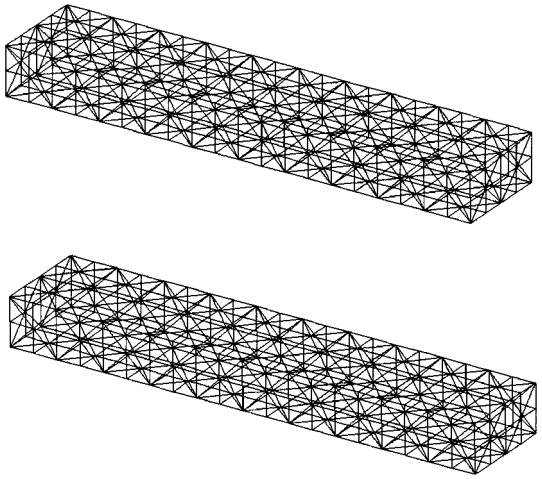

Fig. 8. Example: clamped 100 × 20 × 0.5 μm fixed-fixed beam with zero residual stress suspended 2 μm above an equal-sized fixed electrode.

a wide range of applied voltages. As a practical matter, we can find this quasi-static solution for the macromodel equations by adding damping to the equations of motion and applying a step excitation in the SABER simulator.

We shall use the clamped beam depicted in Fig. 8 for this comparison, and consider only one generalized coordinate, corresponding to the fundamental mode. A negative value for this mode corresponds to the structure bending toward the electrode.

Fig. 12 shows a comparison between the quasi-static modal amplitude obtained from the linearized macromodel and the 3-D quasi-static coupled electromechanical simulation with CoSolve-EM. We observe that for small voltages and displacements, there is good agreement, but when the displacement approaches about half the beam thickness of 0.5 μm, there are substantial departures. The actual structure appears much stiffer

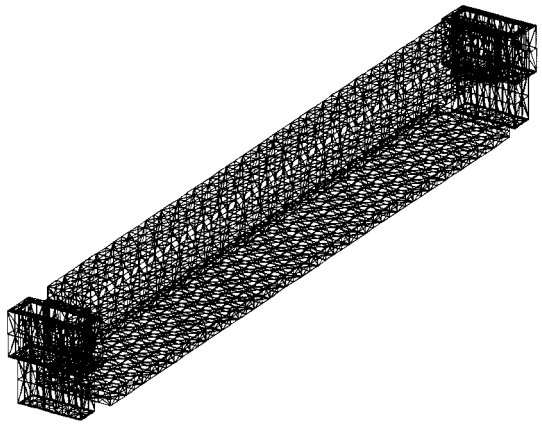

Fig. 9. Example: prestressed 600 × 40 × 2 μm fixed-fixed beam with compliant supports and an initial compressive stress of 4 MPa suspended 2 μm above an equally sized fixed electrode.

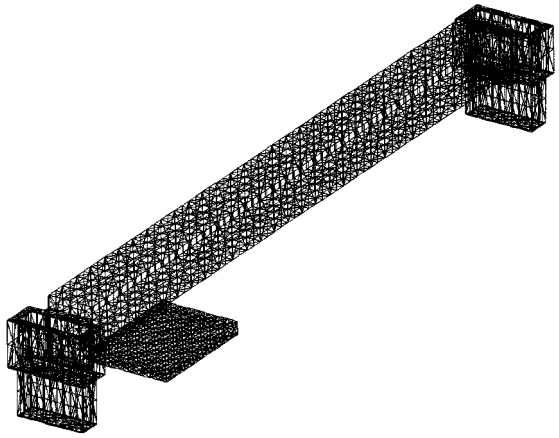

Fig. 10. Example: 600 × 40 × 2 μm fixed-fixed beam with zero residual stress, suspended 2 μm above a 70 × 100 μm electrode that is located lengthwise under the beam, 80 μm away from the near support.

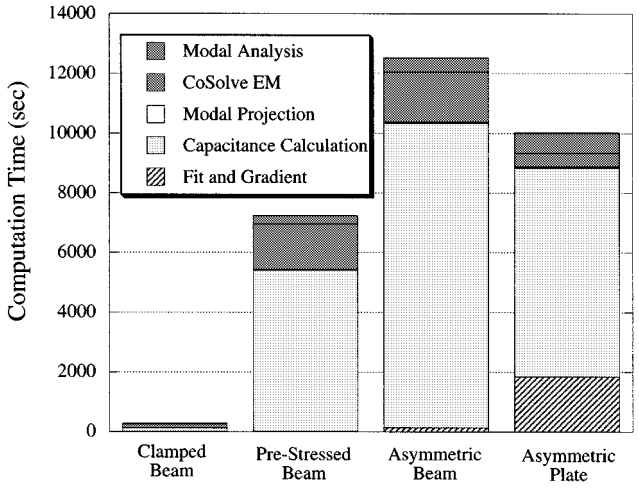

Fig. 11. Summary of computation times for examples.

than the linear macromodel. This is because as the clamped beam bends, it must get longer. Thus, there is an axial stress that must accompany bending, and the elastic stored energy as a result of this axial extension adds to the overall stiffness of the

TABLE III
SUMMARY OF RESULTS FOR EXAMPLES

Example Information	Clamped Beam	Pre-Stressed Beam	Asymmetric Beam	Asymmetric Plate
Nodes (N)	534	2664	2863	2814
Calculated modes (m')	3	16	30	30
Selected modes (m)	1	3	3	5
CoSolve-EM Actuation voltage as fraction of pull-in	0.81	0.99	0.97	0.61
Capacitance calculations	20	100	200	250
Polynomial coefficients	9	229	401	863
Computation Times (sec)				
Modal analyisis	22	274	487	696
CoSolve-EM	130	1532	1670	447
Modal projection	2	16	35	37
Capacitance calculation	120	5400	10200	7000
Capacitance fit and gradient	0.05	13	136	1844
Total time for CHURN (hours)	0.2	2.1	3.5	3.0

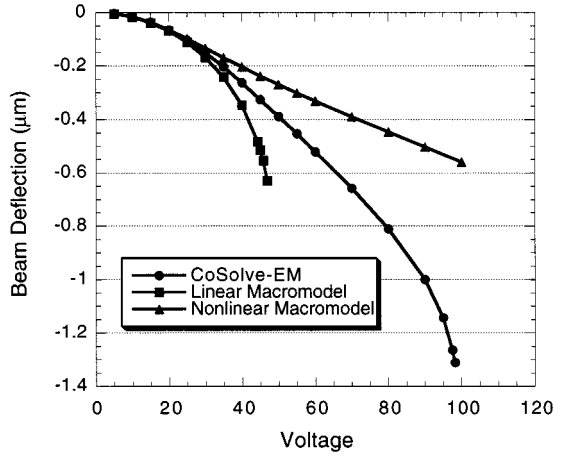

Fig. 12. Comparison of linear and nonlinear macromodels to quasi-static simulation with CoSolve-EM.

structure. This kind of stress-stiffening is a well-known effect in mechanics (see, for example [14]).

It is reasonable to ask whether the same CHURN method that was used for finding the electrostatic co-energy could be used to find an improved representation for the mechanical stored energy, replacing the linearized form of $U_m(q)$ in (10) with a numerically derived analytical function that could be differentiated to yield F_m. The third curve (labeled nonlinear model) in Fig. 12 shows the modal amplitude versus voltage for this case. It is seen that the nonlinear model derived with the CHURN process applied to the elastic energy errs in the opposite direction, producing a macromodel that is much too stiff. We understand the reason for this: the modal displacements used in the electrostatic CHURN process constrain all three degrees of freedom for every node. While this can yield accurate representations for *external* effects, such as capacitance, it can be very incorrect for *internal* effects. For example, when using modal displacements, Poisson contractions are prohibited, and axial displacements that accompany shear during bending are prohibited. As a result, the nodal positions that result from applying a modal displacement are not at their quasi-static equilibrium positions, and this departure from equilibrium creates additional stored elastic energy, increasing the apparent stiffness.

It will be shown in [2] that the CHURN approach can still be used in many cases, but not using the original linearized modes as basis functions for calculating the strain energy. Instead, a slightly modified set of basis functions must be used.

V. CONCLUSIONS

We have presented a method for macromodeling two-conductor electromechanical devices without dissipation, and we have successfully applied this to the electrostatic actuation of a suspended beam and an elastically supported plate with an eccentric electrode and unequal springs. The technique can be extended to more conductors by calculating the complete capacitance matrix as functions of the modal displacements, something that FastCap does quite efficiently. The technique can also be extended to conservative energy domains that are external to the elastic body, such as magnetostatic actuation [12]. However, the method cannot handle dissipative effects, such as fluid damping. When dissipation is present, it is necessary to consider both $\dot{q}$ and q as state variables so the state cannot be evaluated quasi-statically. One promising approach is the use of a small number of explicitly calculated dynamical transients, from which basis functions are extracted empirically [15], [16].

An important benefit of the automated macromodeling approach presented here is that it minimizes the number of iterative (time-consuming) self-consistent coupled simulations that must be performed. A single such simulation is used to get estimates of the size of the modal work space, but all simulations thereafter are single energy domain, hence, fast. Further, as an aid to the designer, the macromodel is automatically exported as a circuit-simulator network element.

Finally, we note that the most complex design studied here only required a few hours for complete construction of the macromodel (after meshing). This means that a designer could create the design, and within one day evaluate the dynamical performance of the device in a feedback loop. This appears to be a very useful step toward speeding up the overall design process without sacrificing accuracy.

ACKNOWLEDGMENT

This work was performed while the authors were at the Microsystems Technology Laboratories, Massachusetts Institute of Technology, Cambridge. The authors wish to thank Microcosm Technologies for extensive cooperation in interfacing MEMCAD 3.2 with the macromodeling tools developed here.

REFERENCES

[1] S. D. Senturia, "CAD challenges for microsensors, microactuators, and microsystems," *Proc. IEEE*, vol. 86, pp. 1611–1626, Aug 1998.

[2] J. E. Mehner, L. D. Gabbay, and S. D. Senturia, "Computer-aided generation of nonlinear reduced-order dynamic macromodels—II: Stress-stiffened motion," *J. Microelectromechanical Systems*, vol. 9, pp. 270–278, June 2000.

[3] S. D. Senturia, "CAD for microelectromechanical systems," in *Proc. Int. Solid-State Sensors Actuators Conf.*, vol. 2, Stockholm, Sweden, June 25–29, 1995, pp. 5–8.

[4] S. D. Senturia, N. Aluru, and J. White, "Simulating the behavior of MEMS devices: computational methods and needs," *IEEE Comput. Sci. Eng. Mag.*, vol. 4, pp. 30–43, Jan. 1997.

[5] L. D. Gabbay, "Computer-aided macromodeling for MEMS," Ph.D. dissertation, Dept. Elect. Eng. Comput. Sci., Massachusetts Inst. Technol., Cambridge, MA, 1998.

[6] H. Goldstein, *Classical Mechanics*, 2nd ed. Reading, MA: Addison-Wesley, 1981, pp. 16–21.

[7] L. Meinorovitch, *Analytical Methods in Vibrations*. New York: Macmillan, 1967.

[8] H. A. Haus and J. R. Melcher, *Electromagnetic Fields and Energy*. Englewood Cliffs, NJ: Prentice-Hall, 1989.

[9] G. K. Ananthasuresh, R. K. Gupta, and S. D. Senturia, "An approach to macromodeling of MEMS for nonlinear dynamic simulation," *Microelectromech. Syst.*, ser. ASME Dynamic Systems and Control (DSC) Series, vol. 59, pp. 401–407, 1996.

[10] J. Stöer and R. Bulirsch, *Introduction to Numerical Analysis*, 2nd ed. Berlin, Germany: Springer-Verlag, 1992.

[11] W. H. Press and S. A. Teukolsky *et al.*, *Numerical Recipes in C: The Art of Scientific Computing*, 2nd ed. Cambridge, U.K.: Cambridge Univ. Press, 1995, pp. 681–688.

[12] M. Varghese, V. L. Rabinovich, and S. D. Senturia, "Reduced-order modeling of Lorentz force actuation with modal basis functions," in *Proc. Modeling and Simulation Microsyst. Workshop*, San Juan, Puerto Rico, April 19–21, 1999.

[13] K. Nabors and J. White, "FastCap: Amultipole-accelerated 3-D capacitance extraction program," *IEEE Trans. Computer-Aided Design*, vol. 10, pp. 1447–1459, Nov. 1991.

[14] J. S. Przemieniecki, *Theory of Matrix Structural Analysis*. New York: McGraw-Hill, 1968.

[15] E. S. Hung, Y.-J. Yang, and S. D. Senturia, "Low-order models for fast dynamical simulation of MEMS microstructures," in *Proc. Int. Solid-State Sens. Actuators Conf.*, Chicago, June 1997, pp. 1101–1104.

[16] E. S. Hung and S. D. Senturia, "Generating efficient dynamical models for microelectromechanical systems from a few finite-element simulation runs," *J. Microelectromech. Syst.*, vol. 8, pp. 280–289, Sept. 1999.

Lynn D. Gabbay received the B.S. degree in applied physics and computer science from Cornell University, Ithaca, NY, in 1993, and the M.S. and Ph.D. degrees in electrical engineering and computer science from the Massachusetts Institute of Technology, Cambridge, in 1995 and 1998, respectively.

From 1994 to 1998, he performed research in the field of computer-aided macromodeling for MEMS. He is currently an Independent Consultant. His research interests include the design and implementation of automated macromodel construction algorithms, and the integration of these tools into existing system simulators.

Jan E. Mehner received the Diploma and the Dr.-Ing. degree in electrical engineering and information technology from the Chemnitz University of Technology, Chemnitz, Germany, in 1989 and 1994, respectively.

From 1998 to 1999 he was a Visiting Scientist at the Massachusetts Institute of Technology, Cambridge, where he was involved in the field of macromodeling. He is currently a Scientific Assistant in the Department of Microsystems and Precision Engineering, Chemnitz University of Technology. His research interests include analytical and numerical methods to design microsystems, CAD tools, and computational algorithms for problems with coupled fields.

Stephen D. Senturia (M'77–SM'91–F'93) received the B.A. degree in physics (*summa cum laude*) from Harvard University, Cambridge, MA, in 1961, and the Ph.D. degree in physics from the Massachusetts Institute of Technology, Cambridge, in 1966.

Since 1966, he has been with the Massachusetts Institute of Technology, where he is currently the Barton L. Weller Professor of Electrical Engineering. In 1982, he founded Micromet Instruments Inc., and served on its Board of Directors until 1992. His current principal research activities are the development of CAD systems for design and simulation of MEMS devices and the use of microfabricated structures for both microsensor and microactuator applications, and for materials research.

Dr. Senturia is a member of Phi Beta Kappa and Sigma Xi. He is a trustee of the Transducer Research Foundation. He is a founding associate editor of the JOURNAL OF MICROELECTROMECHANICAL SYSTEMS (since 1992), and currently serves as a senior editor. He was the solid-state sensors associate editor of the IEEE TRANSACTIONS ON ELECTRON DEVICES (1985–1996) and has been an active participant in the organization and planning of major conferences on solid-state sensors and actuators since 1983. He is corecipient of an IR-100 Award for his work on automated reclamation of urban solid waste, and of the 1988 Arthur K. Doolittle Prize of the Division of Polymeric Materials Science and Engineering of the American Chemical Society.